IJE TRANSACTIONS B: Applications Vol. 39, No. 05, (May 2026) 1152-1160

International Journal of Engineering

Journal Homepage: www.ije.ir

Evaluation of Efficiency of Associated Petroleum Gas Utilization under Conditions of Low Atmospheric Humidity

A. V. Mysin*[a], M. V. Bykova[b], E. E. Soloveva[c]

[a] *Empress Catherine II Saint Petersburg Mining University, Drilling Department, Saint Petersburg, Russia*
[b] *Empress Catherine II Saint Petersburg Mining University, Research Center "Assessment of anthropogenic transformation of ecosystems", Saint Petersburg, Russia*
[c] *Empress Catherine II Saint Petersburg Mining University, Department of Geoecology, Saint Petersburg, Russia*

P A P E R I N F O

Paper history:
Received 17 April 2025
Received in revised form 24 June 2025
Accepted 13 July 2025

Keywords:
Associated Petroleum Gas
Numerical Modeling
Amorphous Carbon
Water Vapor
Carbon Dioxide
Nitrogen Oxides

A B S T R A C T

The study is devoted to the analysis of changes in the composition and amount of emissions during the utilization of associated petroleum gas (APG) under conditions of low humidity of the atmospheric air. An analysis of modern methods for assessing pollutant emissions and thermal effects during flaring of APG is presented. For a more complete assessment of the APG flaring process, determining the composition of emissions, flare stability when changing the flow rate and composition of gas due to the introduction of water vapor, a calculation was performed in ANSYS Fluent, which allows simulating the dynamics of liquids and gases (CFD). Numerical studies were performed based on the solution of equations of conservation of mass, momentum, energy and mass transfer of particles. Within the framework of the study, the composition, completeness of combustion (efficiency) were determined by adding water vapor to the combustion zone as one of the ways to reduce the formation of amorphous carbon. A one-step model was used to predict the formation of amorphous carbon. According to the modeling results, it was found that with a water vapor content of about 30%, a reduction in the formation of amorphous carbon, nitrogen oxides and carbon dioxide was observed. The greatest distance of the combustion zone from the torch was observed with the introduction of 10% water vapor. As a result of the study, it was established that the achievement of maximum effective utilization of APG in conditions of low atmospheric humidity occurs with the introduction of 30% water vapor into the combustion zone of the flare burner.

***doi**: 10.5829/ije.2026.39.05b.09*

Graphical Abstract

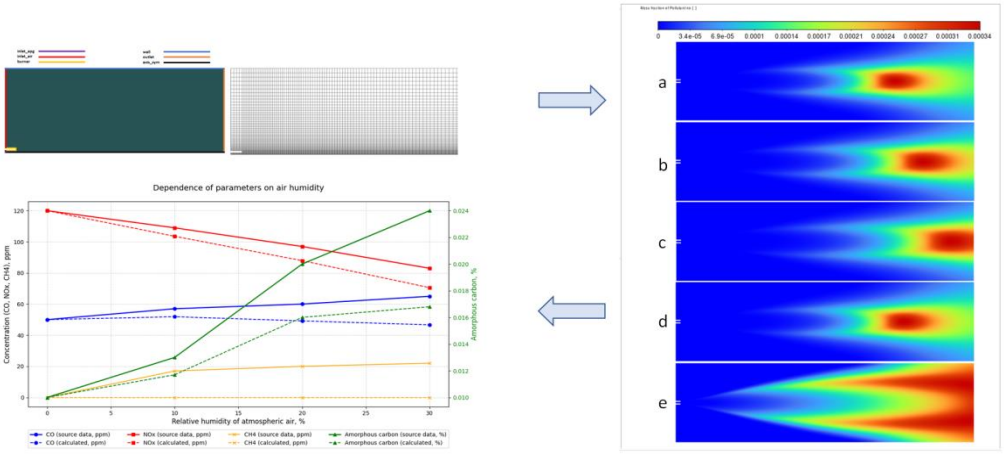

* Corresponding Author Email: *mysin_av@pers.spmi.ru* (A. V. Mysin)

Please cite this article as: Mysin AV, Bykova MV, Soloveva EE. Evaluation of Efficiency of Associated Petroleum Gas Utilization under Conditions of Low Atmospheric Humidity. International Journal of Engineering, Transactions B: Applications. 2026;39(05):1152-60.

NOMENCLATURE

R_i	Rate of formation of chemical reaction products	u	Average speed (m/s)
S_i	Rate of product formation taking into account the addition of the dispersed phase	u'	Pulsation speed (m/s)
N	The total amount of chemical components in the system	k_{eff}	Effective thermal conductivity coefficient
J_i	Diffusion flux of the i- component arising due to the concentration gradient	h	Enthalpy
p	Pressure (Pa)	Y_M	Contribution of fluctuating expansion in compressible turbulence to the total dissipation rate
T	Temperature (K)	$C_1\ C_2\ C_{1\varepsilon}\ C_{3\varepsilon}$	Constants
k	Kinetic energy of turbulence (J/kg)	$S_k\ S_\varepsilon$	User-defined quantities based on initial conditions
G_k	Kinetic energy of turbulent flow	**Greek Symbols**	
G_b	Kinetic energy of a turbulent flow arising from buoyancy	τ	Shear stress tensor
Y_{soot}	Mass fraction of amorphous carbon (%)	ρ	Density (kg/m^3)
R_{soot}	Amorphous carbon formation rate (kg/m^3·s)	ω	Dissipation of turbulent energy (s^{-1})
ε	Specific energy dissipation (W/kg)	$\sigma_k, \sigma_\varepsilon$	Turbulent Prandtl numbers
ν	Kinematic viscosity	μ_t	Turbulent dynamic viscosity

1. INTRODUCTION

Over the past two years, oil production in the world has remained at a consistently high level. In the US, it is 12.9 million barrels per day, in Saudi Arabia and Russia, about 10.5 million barrels per day. This in turn indicates high volumes of recoverable associated petroleum gas. To achieve sustainable development goals, it is necessary to utilize associated petroleum gas with a high degree of efficiency. According to the data presented in Figure 1, it can be noted that in the US, almost all associated petroleum gas is processed or used. In Russia, there is also a significant volume of gas utilization; but in Iraq and Nigeria, there is a low level of utilization (1, 2).

Integrated approaches to solve the problem of increasing the efficiency of APG utilization, taking into account the development of technologies, have led to the creation of a large number of different methods.

The most promising and frequently used include the following: processing into liquid hydrocarbons; injection into the reservoir; power generation; compression and transportation; obtaining LPG; combustion. The last of the above methods still occupies the main share among all those used.

Among the countries of the world, Russia occupies one of the leading positions in hydrocarbon production and is a leader in associated petroleum gas flaring. About 15% of the world's volume of flared gas is accounted for by Russia (3-5).

Large deposits, where the bulk of hydrocarbons are produced, are located in the northern regions of the country and are the main supplier of pollutants into the atmosphere.

However, Russia is not the only one influencing the Arctic region of the planet: the United States of America also considers the Arctic territories as a potential expansion of its borders, including for gaining access to new hydrocarbon deposits.

The Sixth Assessment Report of the United Nations (UN) Intergovernmental Panel on Climate Change (IPCC) for 2021 confirmed that the observed global warming is the most pronounced in the Arctic (6).

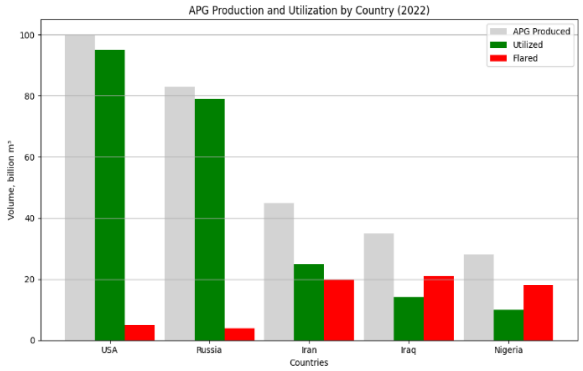

Figure 1. APG production and utilization volumes (3)

This is reflected not only in changes in physical factors such as increased Arctic land and ocean surface temperatures, increased precipitation, reduced snow cover, melting permafrost, and reduced sea ice thickness and extent (Figure 2), but also in increased intensity and frequency of extreme events associated with rapid sea ice loss, melting of the Greenland ice sheet, and wildfires (7).

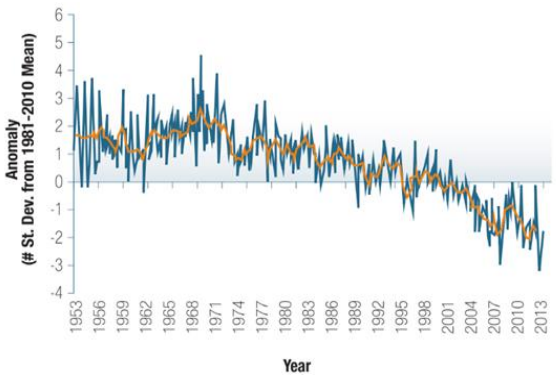

Figure 2. Arctic sea ice extent anomalies (deviations from average) – 1953-2013 (1, 2)

Transformation of the cryosphere due to global warming affects ecosystems across the Arctic, altering productivity, seasonality, distribution and interactions of species in terrestrial, coastal and marine ecosystems (3, 4). This in turn affects the cycling of carbon and greenhouse gases.

One of the causes of climate change is the emission of greenhouse gases or "short-lived climate pollutants", which include amorphous carbon (soot), methane, ozone, hydrogen-containing compounds of fluorine and carbon (8, 9). The main process that results in the largest emission of methane and black carbon into the atmosphere is the combustion process. In the industrial sector, a significant contribution to the release of pollutants into the atmosphere is made by flare flaring of associated petroleum gas (10-12).

According to the Circum-Arctic Resources Assessment Report published by the United States Geological Survey (USGS), the total undiscovered oil and gas resources in the Arctic region account for 22% of the world's total undiscovered oil and gas resources (2). The potential increase in the number of oil fields being developed in low humidity conditions, such as the Arctic region, will certainly exacerbate the problem of global warming. Thus, assessing and reducing greenhouse gas emissions from APG flaring in low humidity conditions is a pressing issue. It should be noted that the main difficulties encountered in quantifying pollutants released into the atmosphere are related to the changing composition of emissions from APG utilization at a flare unit, due to the component composition of the hydrocarbons produced.

The aim of the study is to assess the composition of pollutant emissions during the utilization of associated petroleum gas in conditions of low atmospheric humidity based on numerical modeling.

2. MATERIALS AND METODS

Currently, one of the most widely used methods for assessing emissions of pollutants into the atmosphere during the utilization of APG is satellite monitoring. Earth remote sensing data (hereinafter referred to as ERS) allows for prompt monitoring of the status and number of facilities utilizing APG.

Zhizhin et al. (13) presented an assessment of emissions based on remote sensing with subsequent processing of space images based on the VIIRS Nightfire algorithm. This algorithm relies on the detection of a source signal in the near, mid, and far IR ranges and allows for the recognition and description of “hot spots” on the Earth’s night surface (14). The method recognizes flares as point, stable, high-temperature sources of thermal IR radiation, which allows them to be separated from industrial facilities or natural phenomena. The decoding of daytime images in the near to far IR range by this algorithm is complicated by “noise” from sunlight. In medium-resolution photographs, “hot spots” are not recognized.

A similar algorithm for finding “hot spots” is based on satellite images from the Landsat 8 satellite (15). It is published on the official website of the US Geological Survey and can be implemented using a program in the Python programming language and ArcGIS software tools. The algorithm identifies thermal spots by converting four pre-processed raster images into a vector image representing groupings of pixels with higher brightness that can be interpreted as thermal spots (16).

Another method implemented on the TROPOMI spectrometer (Sentinel-5P satellite) allows indirectly assessing the volumes of APG utilization based on data on the concentrations of some chemicals in the vertical column of the troposphere (17). The TROPOMI spectrometer takes pictures in the ultraviolet, visible, near infrared and mid-infrared ranges of the electromagnetic spectrum (18). Obviously, such approaches require high-quality space images with sufficient resolution. In addition, based on the assessment results, it is possible to obtain the total volume of APG utilization of only some chemicals.

Mathematical methods are also used to assess pollutant emissions. Their advantage lies in the wide variety of implementation methods, for example, using mathematical software, MathCAD or MATLAB, or other similar programs (19). In addition, software from Integral, well known among environmental engineers, allows one to estimate gas emissions from flares (20-22).

For a more complete assessment of the process of utilization of exhaust gases in the flare (completeness of combustion, absence of formation of aldehydes, acids and other intermediate components), determination of the emission composition (including the presence of amorphous carbon) and, accordingly, the stability of the flare when changing the flow rate and composition of the gas, it is recommended to perform calculations in programs that allow modeling the dynamics of liquids and gases (CFD). Three-dimensional mathematical modeling implemented in the ANSYS Fluent program can most clearly implement this task. This software allows you to solve complex and diverse three-dimensional problems about the flow of liquid and gas. ANSYS Fluent implements a number of mathematical models that can be used with the Navier-Stokes equations to describe chemical or physical processes, such as the combustion process.

3. NUMERICAL SIMULATION

The CFD modeling method is based on solving the equations of conservation of mass, momentum, energy

and the equation of mass transfer of particles. Additionally, turbulence models (e.g. SST; RSM) are solved in scalar equations. These equations describe such quantities as: kinetic energy of turbulence (k); dissipation of turbulent energy (ω); specific energy dissipation (ε).

When the mass conservation equations are solved for chemical species, the computational code can predict the local mass of each species by solving the diffusion equation for the i-th species. This mass conservation equation takes the following general form (Equation 1) (23):

$$\frac{\partial}{\partial t}(\rho Y_i) + \nabla \cdot (\rho v Y_i) = -\nabla \cdot J_i + R_i + S_i \quad (1)$$

This equation is solved for n-1 chemical components in the system.

The basic equations that determine the flow field (Equations 2-4):

$$\frac{\partial}{\partial x_i}(\rho u_i) = 0 \quad (2)$$

$$\frac{\partial}{\partial x_i}(\rho u_i u_j) = -\frac{\partial p}{\partial x_i} + \frac{\partial}{\partial x_j}\left[\mu\left(\frac{\partial u_i}{\partial x_j} + \frac{\partial u_j}{\partial x_i} - \frac{2}{3}\delta_{ij}\frac{\partial u_k}{\partial x_k}\right)\right] + \frac{\partial}{\partial x_j}\left(-\overline{\rho u_i' u_j'}\right) \quad (3)$$

$$\frac{\partial}{\partial x_i}\left[u_i\left(\rho\left(h + \frac{1}{2}u_j u_i\right)\right)\right] = \frac{\partial}{\partial x_j}\left[k_{eff}\frac{\partial T}{\partial x_j} + u_i(\tau_{ij})_{eff}\right] \quad (4)$$

The calculation uses a "realizable" k-ε turbulence model. The standard formulation of the k-ε model is well known and has been applied to many problems since it was developed by Launder and Spalding (24-26). The variables to be carried forward are k, the kinetic energy of turbulence, and ε, the specific dissipation, which determines the scale of turbulence.

According to the ANSYS Fluent user manual, the "realizable" k-ε model satisfies certain mathematical constraints on the Reynolds stresses consistent with the physics of turbulent flows. The following expressions are used to calculate the flow velocities (Equations 5 and 6):

$$\frac{\partial}{\partial t}(\rho k) = \frac{\partial}{\partial x_j}\left[\left(\mu + \frac{\mu_t}{\sigma_k}\right)\frac{\partial k}{\partial x_j}\right] + G_k + G_b - \rho\varepsilon - Y_M + S_k \quad (5)$$

$$\frac{\partial}{\partial t}(\rho\varepsilon) = \frac{\partial}{\partial x_j}\left[\left(\mu + \frac{\mu_t}{\sigma_\varepsilon}\right)\frac{\partial \varepsilon}{\partial x_j}\right] + \rho C_1 S\varepsilon - \rho C_2 \frac{\varepsilon^2}{k+\sqrt{v\varepsilon}} + C_{1\varepsilon}\frac{\varepsilon}{k}C_{3\varepsilon}G_b + S_\varepsilon \quad (6)$$

The numerical study of the combustion process of associated petroleum gas was carried out under the condition of complete preliminary mixing with atmospheric air. The geometry of the model under study is shown in Figure 3. To reduce the time spent on the calculation, a two-dimensional axisymmetric formulation was used.

The computational domain is a combustion chamber with a diameter of 400 mm and a length of 1500 mm. The axial line is the x-axis, relative to which the symmetry condition is adopted. To improve the quality of the solution, the finite element mesh was adapted (Figure 4). As can be seen from Figure 4a, the mesh thickening region is performed in the areas of intense chemical reactions at high temperatures. The boundary conditions adopted in the study of the combustion process for the computational model are shown in Figure 4b. The chamber walls (wall), according to the conditions of Garréton and Simonin (27), were assumed to be impermeable and prevent slipping. At the inlet, the velocity and concentration profiles were considered uniform. The turbulence intensity was set equal to 5% for the inlet air and gas flows, respectively. In the outlet channel, zero diffusion flows were assumed for all variables. The effect of viscosity is not taken into account; there are no reactions with the burner material.

The combustion of associated gas was modeled using the Species Transport module of the Fluent solver and the Eddy dissipation model.

The eddy dissipation model uses the dissipation rate of eddies containing reactants and products to determine the combustion reaction rate. The eddy dissipation method in its purest form calculates reaction rates based on turbulent mixing rates. An implicit assumption is that chemical kinetic rates are much higher than turbulent

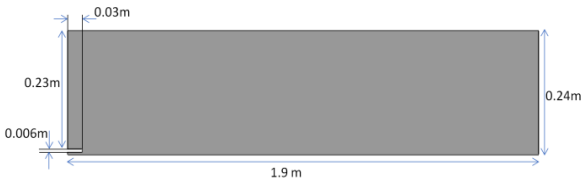

Figure 3. Torch burner

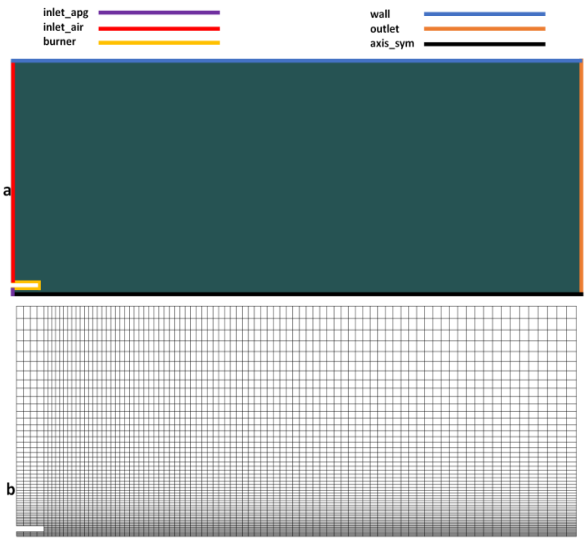

Figure 4. Calculation model: a - boundary conditions; b - grid

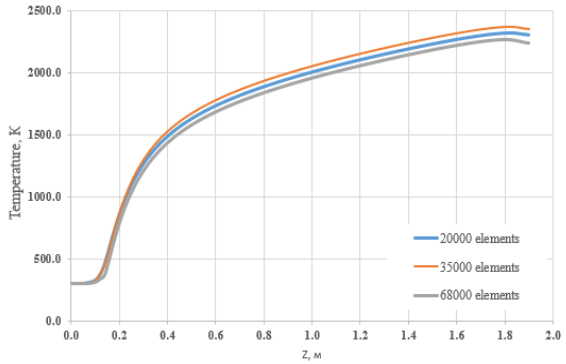

Figure 5. Results of grid convergence testing

mixing rates, i.e., turbulent mixing is the rate-limiting process. This assumption is valid for many combustion processes encountered in practice.

In the calculations, the convergence criterion is set at the level of 10^{-6} for the mass fraction of combustion components, the momentum equation and the continuity equation, and at the level of 10^{-4} for the convergence of the energy conservation equation (28).

Since the grid size is important when using numerical modeling (increasing the number of elements does not always lead to an increase in the accuracy of the solution), a grid independence test was performed. Three different grids were used for this: 1 - 20,000 elements, 2 -35,000 elements, 3 -68,000 elements. The calculation results are shown in Figure 5. The convergence criterion was the change in temperature at different distances from the point of supply of gas, air and water vapor.

As can be seen from Figure 5 in the above, the grid size of 20,000 elements fully satisfies the set tasks of the conducted modeling.

4. RESULTS AND DISCUSSION

The study included determination of the emission composition (formation of amorphous carbon, nitrogen oxides), combustion completeness (efficiency) taking into account the addition of water vapor to the combustion zone (5%, 10%, 20%, 30%) as one of the ways to reduce the formation of amorphous carbon.

4. 1. Analysis of the Combustion Temperature Field The temperature contours during the utilization of APG with the addition of water vapor are shown in Figure 6. It can be seen from the figure that the distribution of the combustion temperature under operating conditions with a mass fraction of water vapor (5%, 10%, 20%, 30%) is approximately the same.

The high temperature region is in the axial direction, and the range remains virtually unchanged, indicating stable combustion. It is also worth noting that the peak

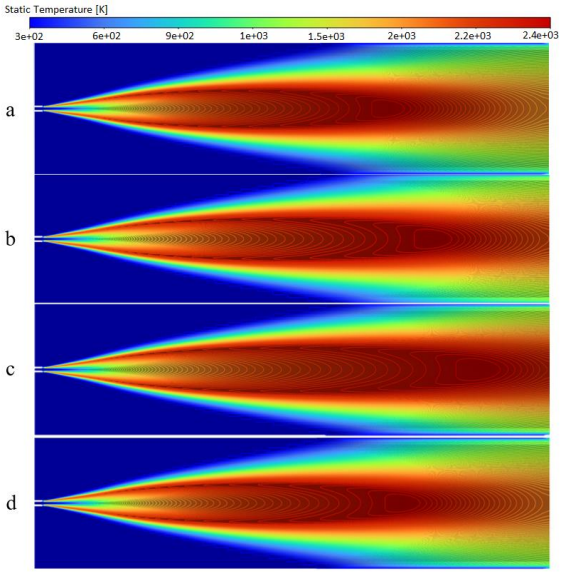

Figure 6. Temperature distribution in the combustion zone with different mass fractions of water vapor (a – 30%; b – 20%, c – 10%; d – 5%)

temperature increases slightly, and the position of the peak area shifts forward under the condition of adding 10% water vapor by mass.

4. 2. Formation of Products as a Result of Utilization of Associated Petroleum Gas

4. 2. 1. Amorphous Carbon Models of amorphous carbon formation can be classified depending on their complexity and the required computational costs. In the work of Kennedy (29), three categories are distinguished: empirical, semi-empirical and detailed models. One of the most well-known empirical models was proposed by Khan et al. (30) to predict emissions of amorphous carbon (soot) in diesel engines and, neglecting particle growth and oxidation rate, allows estimating soot formation as a function of pressure, temperature and equivalence coefficient of unburned gases. A more accurate description of the physics of the process can be obtained using semi-empirical models that take into account the chemical processes involved in soot formation, for example, expressing particle nucleation and surface growth based on the concentration of PAHs.

Zhu et al. (31) used a single-stage model of soot formation, which allows for a fairly accurate prediction of emissions resulting from combustion of associated petroleum gas. For this model, the equation for the transfer of the mass fraction of soot is solved (Equation 7):

$$\frac{\partial}{\partial t}(\rho Y_{soot}) + \nabla \cdot (\rho \vec{v} Y_{soot}) = \nabla \left(\frac{\mu_t}{\sigma_{soot}} \nabla Y_{soot} \right) + R_{soot} \quad (7)$$

The calculation results showed (see Figure 7) that with an increase in the mass fraction of water vapor in the fuel-

air mixture, the formation of amorphous carbon decreases.

4. 2. 2. CO_2 In this work, CO_2 formation was determined through stoichiometric coefficients, enthalpy of formation, and parameters controlling the reaction rate. From the CO_2 formation graphs (Figure 8), it can be concluded that as the water vapor content increases, the combustion efficiency increases and CO_2 formation decreases. That is, when water vapor was not added to the fuel-air mixture, the mass fraction of CO_2 was about 0.145. When the mole fraction of water vapor was 5%, 10%, 20%, and 30%, the mass fraction of CO_2 was 0.144, 0.143, 0.142, and 0.141, respectively.

4. 2. 3. NO_x The main reaction pathways, each with unique characteristics, responsible for the formation of NO_x in combustion processes are:

1. Thermal NO_x, formed as a result of the combination of atmospheric nitrogen and oxygen at high temperatures;
2. Fast-acting NO_x, formed as a result of the reaction of hydrocarbon fragments of the fuel with atmospheric nitrogen at an early stage of the flame front.

Thermal Formation of NO_x:

This mechanism is classified as thermal, due to the strong dependence of the rate of NO_x formation at high temperature (32, 33).

The rate of NO_x formation is determined by the effect of temperature and the residence time of nitrogen at this temperature. Combustion at temperatures below (1300 °C) forms significantly small-scale concentrations of thermal NO_x (34). Usually, at temperatures above this temperature (1600 °C), nitrogen (N_2) and oxygen (O_2) in the air decompose during combustion, taking an atomic form, or enter into successive reactions.

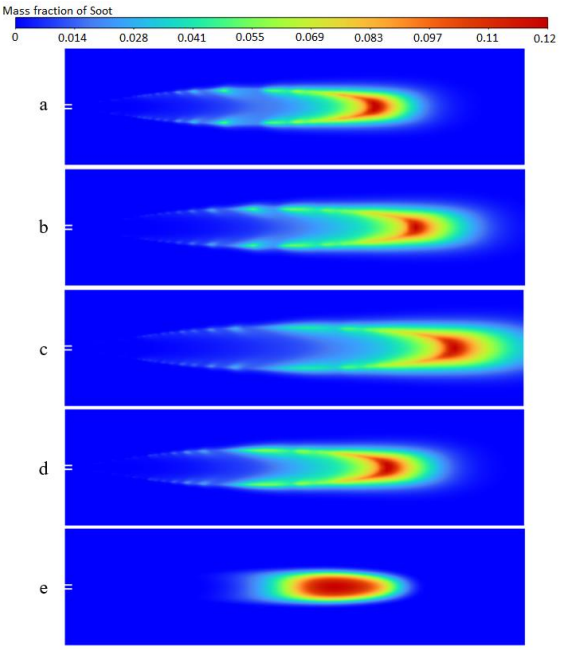

Figure 7. Formation of amorphous carbon at different mass fractions of water vapor (a – 30%; b – 20%, c – 10%; d – 5%; e – 0%)

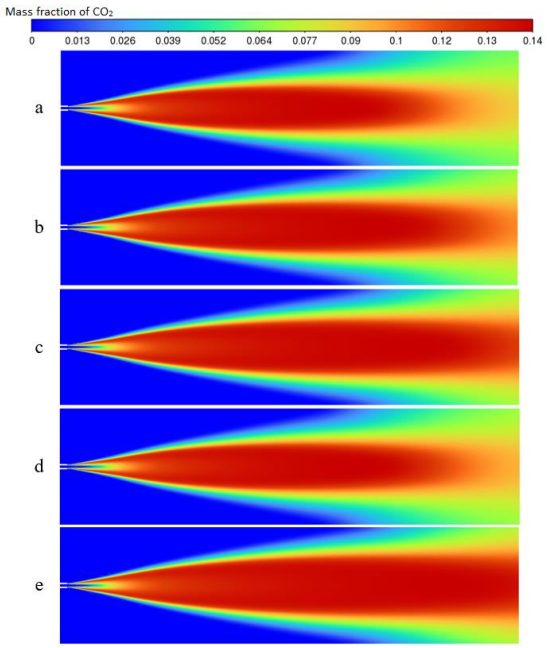

Figure 8. Formation of CO_2 at different mass fractions of water vapor (a – 30%; b – 20%, c – 10%; d – 5%; e – 0%). (Compiled by the authors)

Rapid NO_x formation:

Rapid NO_x formation is proportional to the number of carbon atoms present per unit volume and does not depend on the identity of the original hydrocarbon (35).

The amount of HCN formed increases with increasing concentration of hydrocarbon radicals, which in turn increases with increasing equivalence factor. As the equivalence factor increases, rapid NO_x formation first increases, then reaches a peak, and then decreases due to oxygen deficiency. In this paper, mechanisms 1 and 2 of NO_x formation are used, which allow fairly accurate prediction of emissions from APG utilization.

As can be seen from Figure 9, with an increase in the mass fraction of water vapor in the fuel-air mixture, the content of NO_x pollutants decreases.

According to the simulation results, it was found that with the highest water vapor content (30%), a reduction in the formation of amorphous carbon, nitrogen oxides and carbon dioxide was observed (Figure 10). The greatest distance of the combustion zone from the torch, i.e. a high altitude of pollutant formation, was observed with the introduction of 10% water vapor. In addition, the introduction of 30% water vapor slightly reduces the altitude of the temperature distribution in the combustion zone.

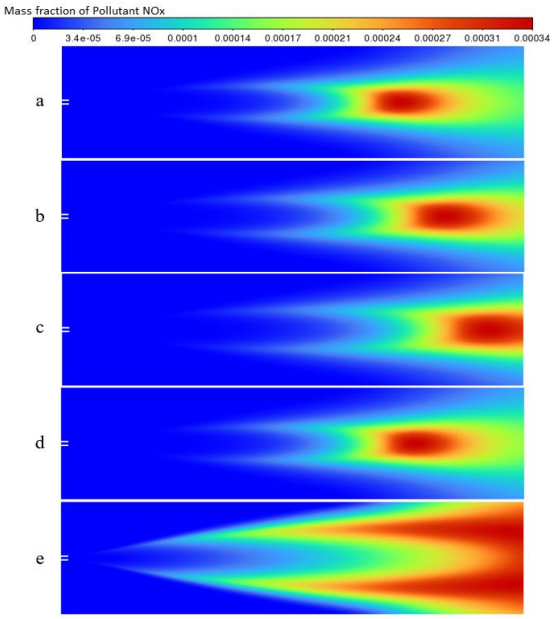

Figure 9. Formation of NOx at different mass fractions of water vapor (a – 30%; b – 20%, c – 10%; d – 5%; e – 0%)

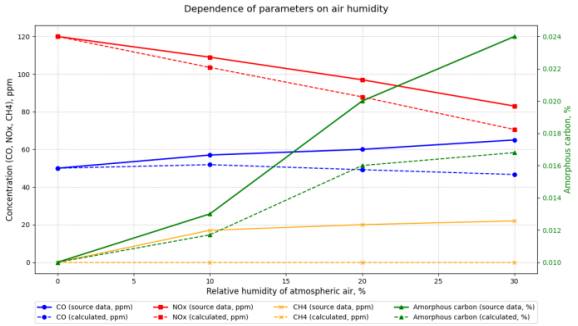

Figure 10. Formation of products during combustion of associated petroleum gas under low humidity conditions without the addition of water vapor (initial) and with different mass fractions of water vapor (calculated)

Thus, the modeling results confirm the fact that the introduction of water vapor into the flare combustion zone makes it possible to reduce the negative impact of APG utilization on the environment, since the completeness, and therefore the quality, of APG combustion increases and the formation of pollutants entering the atmosphere decreases.

The choice of a specific direction for solving the problem of utilization of associated petroleum gas in conditions of low atmospheric humidity can be made on the basis of a comparative analysis of existing methods (Table 1).

However, in the context of modern energy transformation and ESG-oriented agenda, the last three methods of APG utilization are the most promising, but due to the poorly developed infrastructure and remoteness of the hydrocarbon deposits being developed, the method being studied is the most optimal.

TABLE 1. Comparative analysis of the main methods of utilization of associated petroleum gas

Method	Sustainability	Technological complexity	Economic efficiency
Flaring of APG	Low	Low	Low
Flaring of APG (+ 30% water vapor)	Average	Low	Low
Injection into the reservoir	High	High	Low
Electricity generation	Average	High	High
Processing into liquid hydrocarbons	High	High	Average
Compression and transportation	High	Average	Average

5. CONCLUSIONS

Currently, hydrocarbon deposits characterized by low atmospheric humidity, such as those located in the Arctic, are promising regions with significant reserves of hydrocarbon raw materials. However, back in 2021, the UN confirmed that global warming has the greatest impact on the Arctic. Therefore, the tasks associated with reducing emissions of pollutants into the atmosphere, in particular greenhouse gases from the utilization of associated petroleum gas, as the main contributor to "short-lived climate pollutants", are an urgent problem that must be addressed.

As part of this work, an analysis was made of the quantitative change in the composition of greenhouse gases from the utilization of associated petroleum gas for atmospheric air conditions with low humidity, taking into account the addition of water vapor to the combustion zone. Mathematical models were constructed using ANSYS Fluent software.

Before carrying out the calculations, the geometry of the model under study was formed, grid convergence was tested and, in accordance with it, a computational grid was constructed.

The efficiency of fuel-air mixture combustion and pollutant formation were assessed for different mass fractions of water vapor.

6. ACKNOWLEDGMENT

The research was carried out within the state assignment of Ministry of Science and Higher Education of the Russian Federation (FSRW-2023-0002).

7. REFERENCES

1. Masson-Delmotte V, Zhai P, Pirani A, Connors SL, Péan C, Berger S, et al. Summary for policymakers. 2021. 10.1017/9781009157896.001
2. AMAP E. Arctic climate change update 2021: Key trends and impacts. Summary for policy-makers. Tromsø Norway; 2021.
3. Bank W. Global gas flaring reduction partnership (GGFR). 2022.
4. Litvinenko VS, Petrov EI, Vasilevskaya DV, Yakovenko AV, Naumov IA, Ratnikov MA. Assessment of the role of the state in the management of mineral resources. Записки Горного института. 2023(259 (eng)):95-111. 10.31897/PMI.2022.100
5. Cherepovitsyn AE, Tsvetkov PS, Evseeva OO. Critical analysis of methodological approaches to assessing sustainability of arctic oil and gas projects. Записки Горного института. 2021;249:463-78. 10.31897/PMI.2021.3.15
6. Babyr N. Topical themes and new trends in mining industry: Scientometric analysis and research visualization. International Journal of Engineering, Transactions B: Applications. 2024;37(2):439–51. 10.5829/IJE.2024.37.02B.18
7. Secretariat UNFCoCC. United Nations framework convention on climate change: UNFCCC; 1992.
8. Smirnova E, Saychenko L. Hydrodynamic Modeling and Evaluation of Partial Substitution of Cushion Gas During Creation of Temporary Underground Gas Storage in an Aquifer. International Journal of Engineering Transactions A: Basics. 2024;37(07):1221-30. 10.5829/ije.2024.37.07a.02
9. Blinov P, Salakhov K, Nikishin V, Kuchin V. Development of Cement Slurry Composition with Self-healing Properties. International Journal of Engineering, Transactions A: Basics. 2025;38:236-46. https://doi.org/10.5829/ije.2025.38.01a.21
10. Semenova T. Value improving practices in production of hydrocarbon resources in the Arctic regions. Journal of Marine Science and Engineering. 2022;10(2):187. 10.3390/jmse10020187
11. Blinov PA, Sadykov MI, Gorelikov VG, Nikishin VV. Development and research of backfill compounds with improved elastic and strength properties for oil and gas well lining. Записки Горного института. 2024(268 (eng)):588-98.
12. Buslaev G, Morenov V, Konyaev Y, Kraslawski A. Reduction of carbon footprint of the production and field transport of high-viscosity oils in the Arctic region. Chemical Engineering and Processing-Process Intensification. 2021;159:108189. 10.1016/j.cep.2020.108189
13. Zhizhin M, Matveev A, Ghosh T, Hsu F-C, Howells M, Elvidge C. Measuring gas flaring in Russia with multispectral VIIRS nightfire. Remote Sensing. 2021;13(16):3078. https://doi.org/10.3390/rs13163078
14. Elvidge CD, Zhizhin M, Baugh K, Hsu F-C, Ghosh T. Methods for global survey of natural gas flaring from visible infrared imaging radiometer suite data. Energies. 2015;9(1):14. https://doi.org/10.3390/en9010014
15. Landsat U. Landsat 8-9 collection 2 (c2) level 2 science product (l2sp) guide. United States Geological Survey: Asheville, NC, USA. 2022:1-42.
16. Anejionu OC, Blackburn GA, Whyatt JD. Detecting gas flares and estimating flaring volumes at individual flow stations using MODIS data. Remote Sensing of Environment. 2015;158:81-94. https://doi.org/10.1016/j.rse.2014.11.018
17. Veefkind JP, Aben I, McMullan K, Förster H, De Vries J, Otter G, et al. TROPOMI on the ESA Sentinel-5 Precursor: A GMES mission for global observations of the atmospheric composition for climate, air quality and ozone layer applications. Remote sensing of environment. 2012;120:70-83. https://doi.org/10.1016/j.rse.2011.09.027
18. Ialongo I, Stepanova N, Hakkarainen J, Virta H, Gritsenko D. Satellite-based estimates of nitrogen oxide and methane emissions from gas flaring and oil production activities in Sakha Republic, Russia. Atmospheric Environment: X. 2021;11:100114. https://doi.org/10.1016/j.aeaoa.2021.100114
19. Palaev A, Fuming Z. A Leak Detection Method for Underground Polyethylene Gas Pipelines Using Simulation Software Ansys Fluent. International Journal of Engineering Transactions B: Applications. 2024;37(8):1615-21. 10.5829/ije.2024.37.08b.14
20. Nwosisi M, Oguntoke O, Taiwo A. Dispersion and emission patterns of NO2 from gas flaring stations in the Niger Delta, Nigeria. Modeling earth systems and environment. 2020;6(1):73-84. https://doi.org/10.1007/s40808-019-00658-z
21. Strizhenok AV, Ivanov AV. Monitoring of air pollution in the area affected by the storage of primary oil refining waste. Journal of Ecological Engineering. 2021;22(1):60-7. https://doi.org/10.12911/22998993/128873
22. Mysin A, Kovalevskiy V, Kirkin A, editors. Ensuring environmental safety of massive explosions in the combined development of coal deposits in Kuzbass. IOP Conference Series: Earth and Environmental Science; 2021: IOP Publishing.
23. Anderson JD, Wendt J. Computational fluid dynamics: Springer; 1995.
24. Noor M, Wandel AP, Yusaf T, editors. Detail guide for CFD on the simulation of biogas combustion in bluff-body mild burner. Proceedings of the 2nd International Conference on Mechanical Engineering Research (ICMER 2013); 2013: University of Southern Queensland.
25. Paul C, Haworth DC, Modest MF. A simplified CFD model for spectral radiative heat transfer in high-pressure hydrocarbon–air combustion systems. Proceedings of the Combustion Institute. 2019;37(4):4617-24. 10.1016/j.proci.2018.08.024
26. Shi Y, Zhong W, Chen X, Yu A, Li J. Combustion optimization of ultra supercritical boiler based on artificial intelligence. Energy. 2019;170:804-17. 10.1016/j.energy.2018.12.172
27. Garréton D, Simonin O, editors. Aerodynamics of steady state combustion chambers and furnaces. ASCF Ercoftac Cfd Workshop; 1994.
28. Perrone D, Castiglione T, Klimanek A, Morrone P, Amelio M. Numerical simulations on Oxy-MILD combustion of pulverized coal in an industrial boiler. Fuel Processing Technology. 2018;181:361-74. 10.1016/j.fuproc.2018.09.001
29. Kennedy IM. Models of soot formation and oxidation. Progress in Energy and Combustion Science. 1997;23(2):95-132.
30. Khan I, Greeves G, Probert D. Prediction of soot and nitric oxide concentrations in diesel engine exhaust. Air Pollution Control in Transport Engines C. 1971;142:205-17.
31. Zhu Q, Niu Y, Chen X. Impact of water vapor on the soot formation in the laminar methane/air diffusion flame. J Saf Environ. 2017;17:174-7. 10.1016/j.combustflame.2013.12.017
32. Zeldvich YB. The oxidation of nitrogen in combustion and explosions. J Acta Physicochimica. 1946;21:577.
33. Chen Z, Li Z, Zhu Q, Jing J. Gas/particle flow and combustion characteristics and NOx emissions of a new swirl coal burner. Energy. 2011;36(2):709-23. 10.1016/j.energy.2010.12.037
34. Fenimore CP, editor Formation of nitric oxide in premixed hydrocarbon flames. Symposium (international) on combustion; 1971: Elsevier.
35. Zhao L, Wang T, editors. Simulation of combustion and thermal-flow inside a pyroscrubber. ASME International Mechanical Engineering Congress and Exposition; 2009.

Persian Abstract

چکیده

این مطالعه به تجزیه و تحلیل تغییرات در ترکیب و میزان انتشار گازهای گلخانه ای در طول استفاده از گاز نفتی مرتبط در شرایط رطوبت پایین هوای جوی اختصاص داده شده است .تجزیه و تحلیل روش های مدرن برای ارزیابی انتشار آلاینده ها و اثرات حرارتی در طول شعله ور شدن گاز نفتی مرتبط ارائه شده است .برای ارزیابی کامل تر فرآیند شعله ور شدن گاز نفتی مرتبط ، تعیین ترکیب انتشار گازهای گلخانه ای ، ثبات شعله ور شدن هنگام تغییر سرعت جریان و ترکیب گاز به دلیل معرفی بخار آب ، محاسباتی در Ansys Fluent انجام شد که امکان شبیه سازی دینامیک مایعات و گازها را فراهم می کند .مطالعات عددی بر اساس حل معادلات حفظ جرم ، حرکت ، انرژی و انتقال جرم ذرات انجام شد .در چارچوب مطالعه ، ترکیب ، کامل بودن احتراق) کارایی (با اضافه کردن بخار آب به منطقه احتراق به عنوان یکی از راه های کاهش تشکیل کربن بی شکل تعیین شد .یک مدل یک مرحله ای برای پیش بینی تشکیل کربن بی شکل استفاده شد .با توجه به نتایج مدل سازی ، مشخص شد که با محتوای بخار آب حدود 30٪ ، کاهش تشکیل کربن بی شکل ، اکسید نیتروژن و دی اکسید کربن مشاهده شد .بیشترین فاصله منطقه احتراق از شعله ور ، یعنی بیشترین ارتفاع تشکیل آلاینده ، با معرفی 10 ٪ بخار آب مشاهده شد .در نتیجه این مطالعه مشخص شد که دستیابی به حداکثر استفاده موثر از گاز نفتی مرتبط در شرایط رطوبت کم اتمسفر با وارد کردن 30 ٪ بخار آب به منطقه احتراق مشعل رخ می دهد.